# Study of Head-Tape Interaction in High Speed Rotating Head Recording

The steady state tape dynamics resulting from the interaction of a high speed rotating head and a flexible recording tape are formulated within the framework of linear shell theory. Tape displacements in the area above the head are coupled with the solution to the Reynolds equation in order to calculate the film thickness (flying height) between head and tape. Simulated results for spherical heads are compared to observed behavior on experimental systems.

#### Introduction

Rotating head recording with stationary or slowly moving magnetic media first appeared in connection with video recording and later in digital recording systems, such as IBM's 3850 product [1]. Because the rotating head can be moved at a much higher velocity than a spool of tape, significantly higher data rates can be achieved with these systems. However, due to the high relative speed between head and tape, contact between the two surfaces could be catastrophic. In order to achieve high reliability with these high speed systems, it is necessary to have the head and magnetic medium (tape) separated by an air film large enough to prevent contact, but small enough to allow high density magnetic information to be written onto, or read from, the medium.

Observations of high speed rotating head systems [2, 3] have led to the conclusion that the tape response is highly dynamic and, unless stabilizing mechanisms are provided, waves in the tape due to the traveling head will interfere with the head-tape separation (flying height). In a paper by Bogy, Greenberg, and Talke [4], the dynamic response of a cylinder subjected to a moving load was formulated using linear shell theory with the assumption of inextensibility. While this formulation qualitatively predicted the wave behavior and critical speed phenomenon observed in the tape, the inextensibility assumption (bending without extension) led to a strong dependence in the solution on physical dimensions and head speed, and this has not been observed in actual systems. The inextensible solution also predicted, for higher speeds,

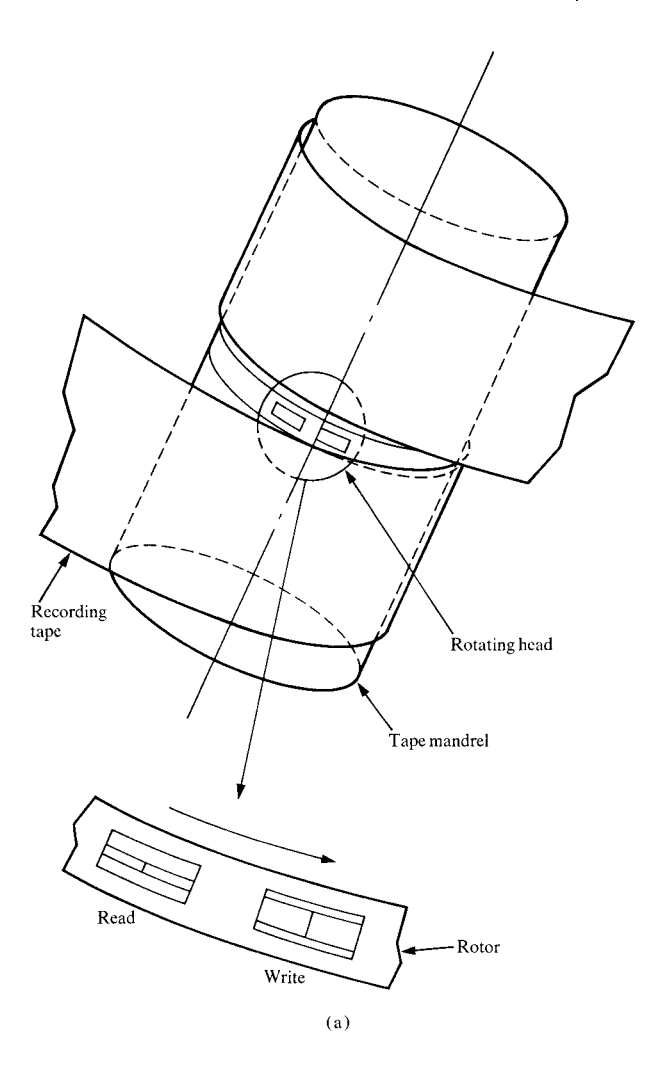
more disparity between the amplitudes and wavelengths of the leading and trailing waves than has been reported [2, 3]. Finally, the model employed in [4] assumed simple supports at some distance (greater than the mandrel gap length [3]) in order to approximate the actual boundary conditions. Since these conditions are not actually met in rotating head configurations, it is desirable that the solution be somewhat insensitive to the distance between supports; however, the inextensible solution in [4] was very sensitive to this parameter.

In this paper, we reformulate the tape dynamics problem by removing the inextensibility assumption and then use the tape deflection in the area immediately above the recording head, together with the pressure profile obtained from the Reynolds equation, in a foil bearing simulation of the tape-head interface.

# Formulation of the tape dynamics [5]

The model for the tape dynamics is the same as that given in [4], i.e., a circumferentially moving load on a simply supported cylindrical shell; the system configuration is shown in Fig. 1(a), and the geometry and loading of the shell are shown in Fig. 1(b). While simple support boundary conditions are still employed in this model for mathematical convenience, it is expected that the removal of the inextensibility assumption will also remove the sensitivity to the distance between the supports. The cylindrical shell equations are used to express the dimensionless displacements for steady motion in coordinates

Copyright 1979 by International Business Machines Corporation. Copying is permitted without payment of royalty provided that (1) each reproduction is done without alteration and (2) the *Journal* reference and IBM copyright notice are included on the first page. The title and abstract may be used without further permission in computer-based and other information-service systems. Permission to *republish* other excerpts should be obtained from the Editor.



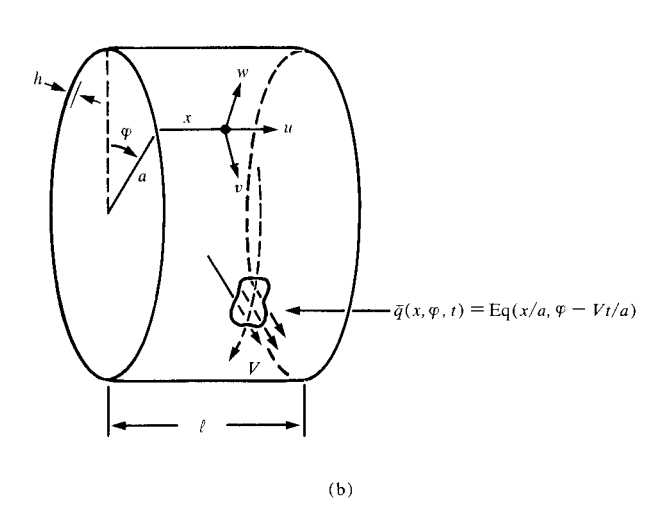


Figure 1 (a) Rotating head system configuration (taken from Fig. 5 of Reference [1], copyright 1975 by the IEEE; reprinted with permission). (b) Geometry and loading for the cylindrical shell.

that move with the load; these can be written in the form

$$\begin{split} u_{\xi\xi} + \nu_2 u_{\phi\phi} + \nu_1 v_{\xi\phi} + \nu_T w_{\xi} &= 0, \\ v_1 u_{\xi\phi} + \nu_2 v_{\xi\xi} + v_{\phi\phi} + w_{\phi} &= 0, \\ v_T u_{\xi} + v_{\phi} + w + k (w_{\xi\xi\xi\xi} + 2w_{\xi\xi\phi\phi} + w_{\phi\phi\phi\phi}) \\ &+ (\bar{V}^2 - T/D) w_{\phi\phi} - \gamma \bar{V} w_{\phi} &= q(\xi, \phi), \end{split} \tag{1}$$

in which Greek subscripts refer to partial differentiation,

$$\begin{split} \phi &= \varphi - Vt/a, \, \xi = x/a, \\ u, \, v, \, w(\xi, \, \phi) &= [h/a^2(1 - \nu^2)][\bar{u}, \, \bar{v}, \, \bar{w}(x, \, \varphi, \, t)], \\ q(\xi, \, \phi) &= \bar{q}(x, \, \varphi, \, t)/E, \, \bar{V} = V/[E/(1 - \nu^2) \, \rho]^{1/2}, \\ k &= h^2/12a^2, \, D = Eh/(1 - \nu^2), \\ \gamma &= ca/\{\rho h[E/(1 - \nu^2) \, \rho]^{1/2}\}, \\ \nu_1 &= (1 + \nu)/2, \, \nu_2 = (1 - \nu)/2, \, \nu_T = \nu - T/D, \end{split}$$

where h, a,  $\nu$ , E, and  $\rho$  represent shell thickness, shell radius, Poisson's ratio, Young's modulus, and density, respectively, while V denotes the speed of the head, c the coefficient of damping, and T the tension in the circumferential direction.

The solution procedure for calculation of the displacements u, v, and w is similar to that employed in [4]; however, considerable complexity is added by the removal of the inextensibility assumption. Proceeding in a manner similar to [4], we obtain the formal solution for radial displacement of the tape,

$$w(\xi, \phi) = \sum_{m=-\infty}^{\infty} \sum_{m=1}^{\infty} W_m(\phi + 2n\pi) \sin \frac{m\pi a}{\ell} \xi, \qquad (2)$$

where  $\ell$  is the distance between assumed simple supports. Here,  $W_m$  is defined in terms of the Fourier inversion integral

$$\begin{split} W_{m}(\theta) &= \frac{1}{2\pi} \\ &\times \int_{-\infty}^{\infty} \frac{\left[ -\nu_{2}p^{4} + (\nu_{1}^{2} - \nu_{2}^{2} - 1)\lambda_{m}^{2}p^{2} - \nu_{2}\lambda_{m}^{4}\right] \tilde{Q}_{m}(p)e^{-ip\theta}dp}{-\nu_{2}k \prod_{j=1}^{8} \left[ p - p_{m}^{(j)} \right]} \,, \end{split}$$
 (3)

where  $\lambda_m = m\pi a/\ell$ ,  $\bar{Q}_m$  is the Fourier transform of the mth mode of the applied load, and  $p_m^{(j)}$ ,  $j = 1, \dots, 8$ , are the roots of an 8th order polynomial. The location of these roots in the p plane together with the appropriate inversion path is shown in Fig. 2.

In the evaluation of the integral by residue theory, the proper contour will encircle the roots in the upper half plane for  $\theta < 0$  and will encircle the roots in the lower half plane for  $\theta > 0$ . Since the distance of a root from the

horizontal axis is an indication of its effective damping in the solution, it can be seen that roots  $p_m^{(3)}$ ,  $p_m^{(4)}$ ,  $p_m^{(5)}$ , and  $p_m^{(6)}$ are the main contributors to the far field dynamic solution. Also, increased distance from the vertical axis is associated with shorter wavelengths, so it can be seen, for the case depicted, that the wavelengths leading the head  $(\theta > 0)$  are shorter than those trailing the head  $(\theta < 0)$ . Fig. 3 shows a root locus in the p plane corresponding to increasing velocity values, and we see that for low velocity the solution is symmetric about  $\theta = 0$  and decays rapidly in  $\theta$ . As velocity is increased, the poles above and below the real axis approach the axis and almost coalesce at a "critical speed" (the poles would exactly coalesce if the damping coefficient were zero). As the speed increases beyond the critical speed, the wavelengths leading the head become shorter while those following become longer. Also, above the critical speed the waves show less tendency to dampen out.

The wave behavior of the tape and the effect of passing through the critical speed as given by the solution to Eq. (2) may be seen from Fig. 4. Figure 4(a) shows the low speed (subcritical) tape response, and Fig. 4(b) shows the high speed (supercritical) response for a dome-shaped pressure distribution over the rotating head. Figure 5 shows capacitance probe traces taken from an actual rotating head device. Comparing Figs. 4 and 5, we see that both our tape model and the actual deflections display a static-like behavior at low speed, a critical speed above which waves exist, and an antisymmetric wave behavior with slightly shorter wavelengths leading the head than trailing the head at high speeds. The deflections calculated from this model have been found to agree very well with observed deflections for both low and high speed (see also the actual deflections presented in [2] and [3]). Thus, we believe that the dynamic shell analysis presented here gives the proper deflections for a wide range of system configurations and is the appropriate analysis to use in a foil bearing simulation of the rotating head-tape interface.

## Reynolds equation

Considering slip flow due to molecular effects, one may write the steady state Reynolds equation for gas-lubricated hydrodynamic bearings [6] in the form

$$\frac{\partial}{\partial \phi} \left[ PH^3 \frac{\partial P}{\partial \phi} \right] + \frac{\partial}{\partial \xi} \left[ PH^3 \frac{\partial P}{\partial \xi} \right] 
+ 6m \left\{ \frac{\partial}{\partial \phi} \left[ H^2 \frac{\partial P}{\partial \phi} \right] + \frac{\partial}{\partial \xi} \left[ H^2 \frac{\partial P}{\partial \xi} \right] \right\} = \Lambda \frac{\partial}{\partial \phi} [PH]. \quad (4)$$

In Eq. (4),

m =Knudsen number (ratio of mean free path length to minimum spacing),

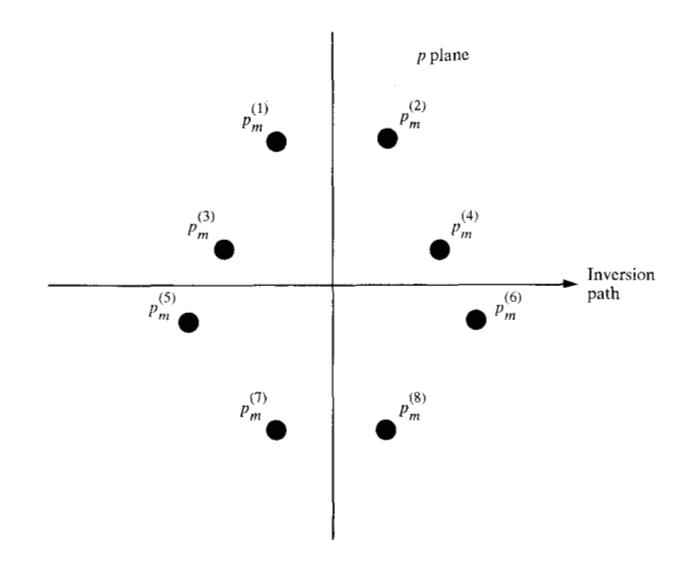


Figure 2 Root locations for Fourier inversion integral.

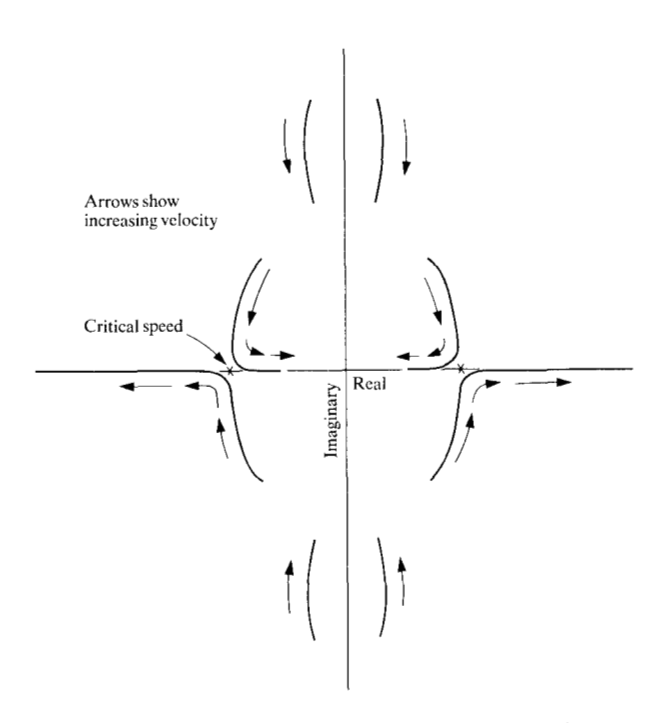


Figure 3 Root locus corresponding to increasing velocity.

 $\Lambda = gas bearing number,$ 

 $H = H(\xi, \phi)$  = the normalized spacing between head and tape, and

$$P = P(\xi, \phi) = 1 + \frac{q(\xi, \phi)}{p_g/E},$$
 (5)

where  $p_{\rm g} = p_{\rm a} + T/a$ ,  $p_{\rm a} =$  ambient pressure, and T =

199

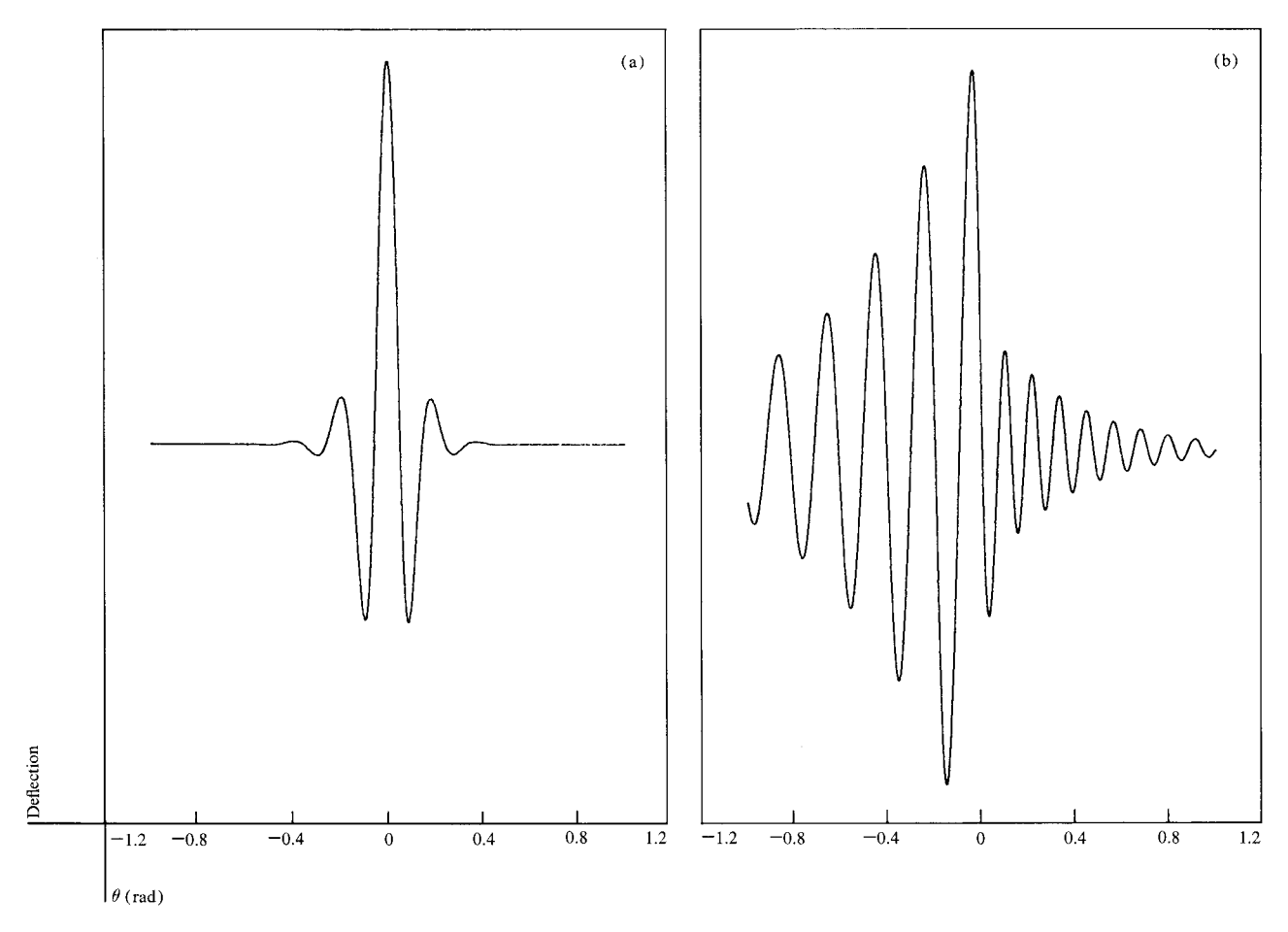


Figure 4 Tape deflection computed from tape dynamics equations: (a) low speed; (b) high speed.

tension. If  $d(\xi, \phi)$  denotes the position of the head with respect to the mandrel, then

$$H(\xi, \, \phi) = \frac{1}{H_{\rm n}} \left[ w(\xi, \, \phi) - d(\xi, \, \phi) \right], \tag{6}$$

where  $H_{\rm n}$  is the nominal spacing. If we assume a spherical contour on the recording head, the head position is given by

$$d(\xi, \phi) = d_0 + a - r + [r^2 - (a\xi - \ell/2)^2 - a^2\phi^2]^{1/2} - a[1 - \phi^2]^{1/2}, \tag{7}$$

where  $d_0$  is the penetration of the center of the head above the mandrel and r is the radius of curvature of the spherical head. Other recording head contours can also be used by either expressing  $d(\xi, \phi)$  analytically or as a matrix of numerical values.

The numerical solution of the Reynolds equation has received considerable attention both in its time dependent form [7] and steady state form [8]. In this paper, the

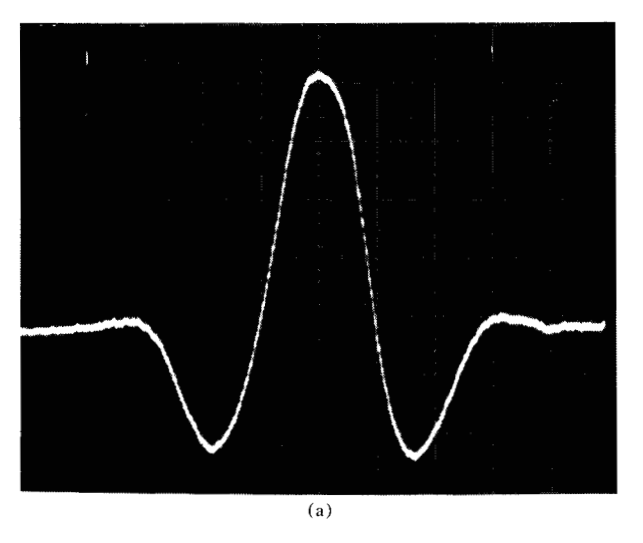
steady state Reynolds equation, Eq. (4), is solved by a relaxation method similar to that described by Michael [8], and the reader is referred to that paper for a discussion of the solution procedure.

#### Coupling

The elastohydrodynamic system describing the interaction between the rotating head and flexible tape requires the simultaneous solution of the tape dynamics equation, which gives the foil deflection for a given pressure distribution, and the Reynolds equation, which gives the pressure distribution necessary to support a given spacing. The coupling procedure involves iterating between the foil deflection calculation and the Reynolds equation until both systems are satisfied by the same values of pressure and spacing.

The coupling procedure developed for the computer solution to this system of equations is summarized in the flow chart of Fig. 6. With  $P_i$  and  $H_i$  the pressure and spacing, respectively, after iteration i, then we use  $H_i$  as input

200



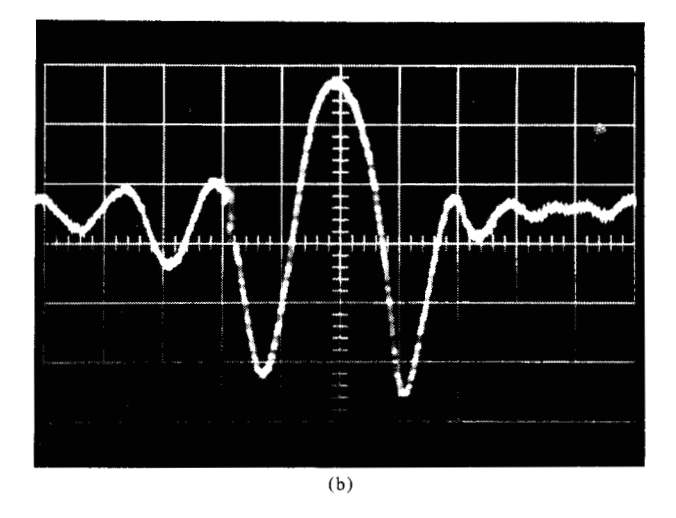


Figure 5 Capacitance probe traces of actual tape deflection: (a) low speed; (b) high speed.

into the Reynolds equation to find the Reynolds pressure  $RP_i$ . Convergence is achieved when

$$\sum_{\text{all grid points}} (RP_i - P_i)^2 < CONV, \tag{8}$$

where *CONV* is the convergence factor. For the next iteration, we form

$$P_{i+1} = P_i + K(RP_i - P_i), (9)$$

where K is a relaxation factor, and then use  $P_{i+1}$  as the input into the foil deflection equation to obtain  $H_{i+1}$ .

To begin execution of the program for a new set of parameters, an initial pressure must be specified. A dome-shaped (cosine-like) pressure of magnitude sufficient to lift the tape over the head provides a convenient point at which to begin iterating. To save time in the iteration scheme, the results from a previous solution with similar parameters may be used to good advantage in the following manner:

- Supply the spacing from the previous solution as input.
- Calculate (from the Reynolds equation) the pressure necessary to support this spacing using current parameter values.
- 3. Use the foil deflection equation to calculate the head-to-tape spacing for this pressure. If this spacing is everywhere positive (no head crash), use the pressure from step 2 as the starting pressure; otherwise, modify the input spacing by decreasing it uniformly (Note: A lower spacing input to the Reynolds equation will result in a higher pressure output), and return to step 2.

During program execution, a quantity called the pressure residual is monitored. The pressure residual is defined by

$$\Delta P_i = (RP_i - P_i)^2,\tag{10}$$

and from Eq. (8) it can be seen that  $\Delta P_i < CONV$  is the convergence criterion. During execution, the pressure residual may not be monotonically decreasing, that is,  $\Delta P_{i+1}$  may be greater than  $\Delta P_i$ . This is to be expected during the early iterations but should be avoided as convergence becomes closer. For this reason, a fine tune factor is used such that if

$$\Delta P_i < TUNE$$
 and if  $\Delta P_{i+1} > \Delta P_i$ ,

then the iteration step is not allowed and a new value of  $P_{i+1}$  is found by a further under-relaxation. That is, the relaxation factor K in Eq. (9) is reduced, and the iteration step is repeated.

The iteration scheme developed here works quite well as long as there is no head crash (negative head-to-tape spacing). Any method of preventing head crashes is acceptable; the one used here is an under-relaxation procedure similar to the fine tune method.

Even though the foil deflection equations and the Reynolds equation are solved separately, the coupling algorithm connects them, and the strong interaction of the two systems requires a small iteration step size (a small value for the relaxation factor *K*) in order to achieve converged values of pressure and spacing which satisfy both systems.

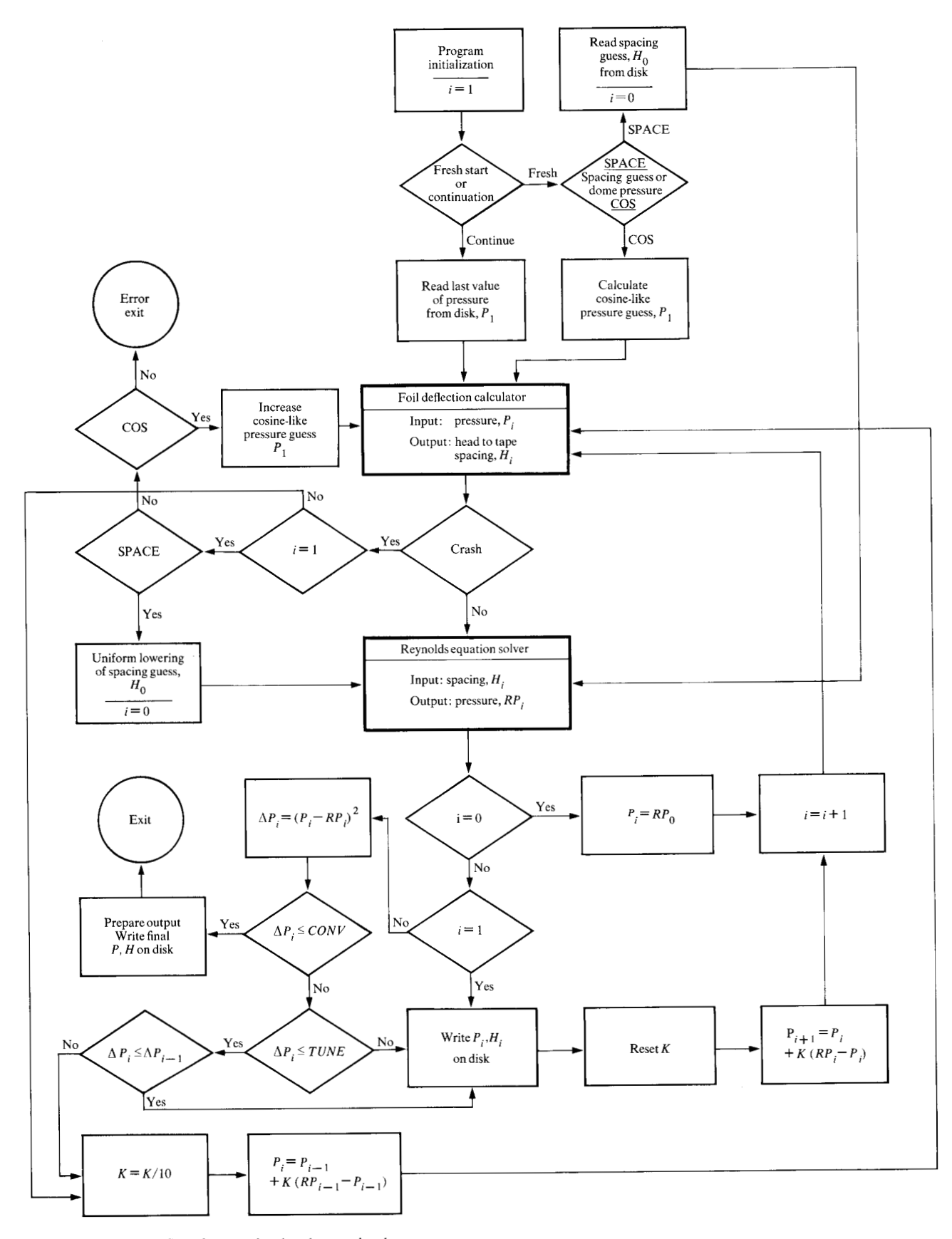
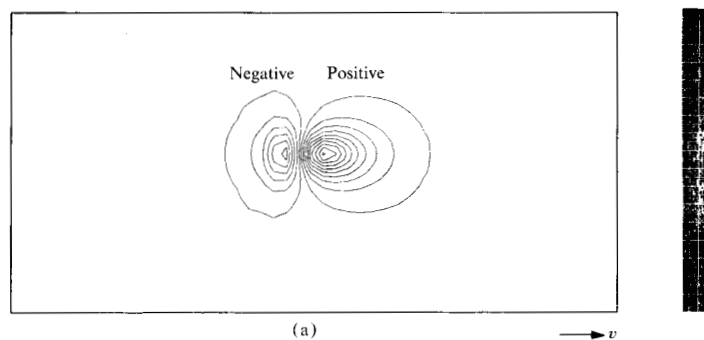


Figure 6 Program flow for rotating head-tape simulator.

202



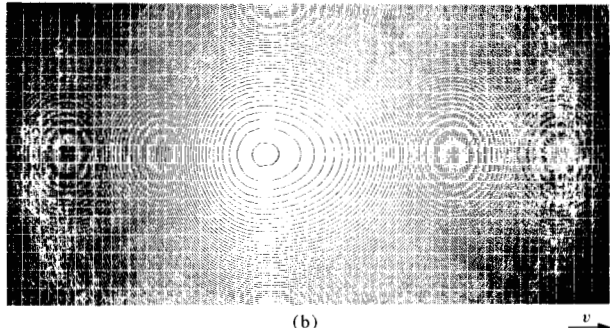
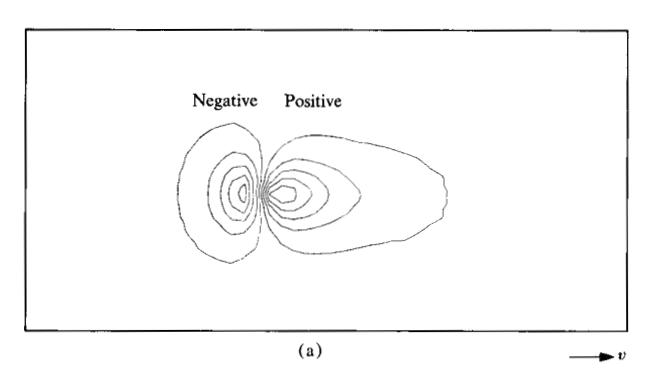


Figure 7 (a) Pressure and (b) spacing for small radius spherical head (19 mm).



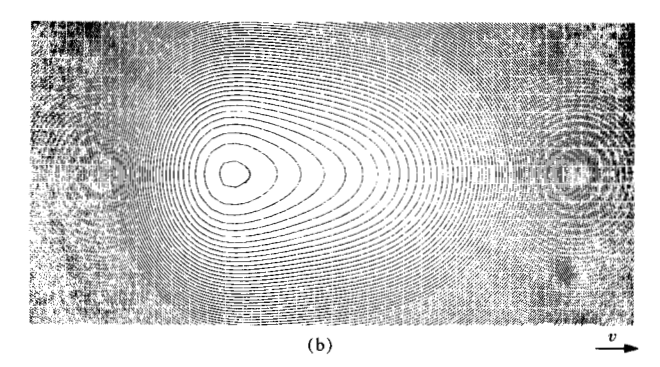
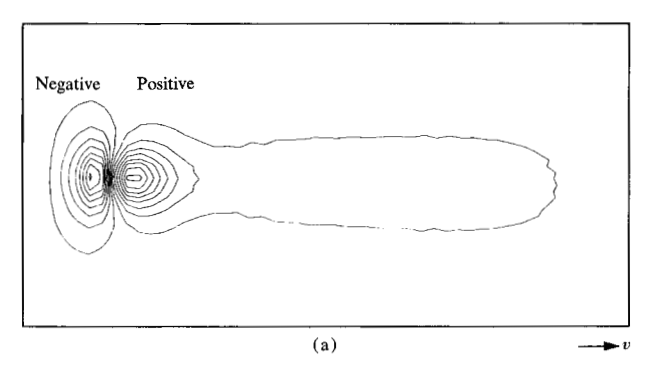


Figure 8 (a) Pressure and (b) spacing for medium radius spherical head (25 mm).



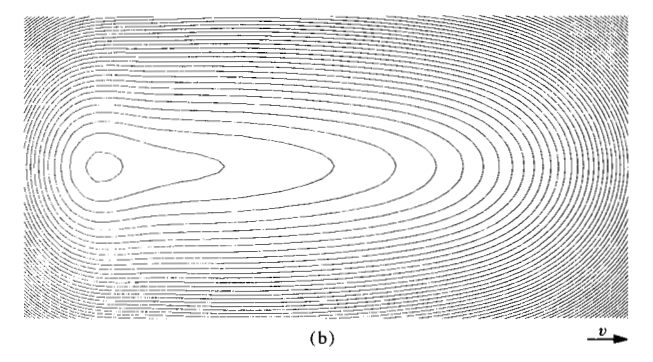


Figure 9 (a) Pressure and (b) spacing for large radius spherical head (32 mm).

### Simulation results and conclusions

Talke and Tseng [9] have presented experimental results for flying heights of several types of heads, including both small radius and large radius spherical heads. They concluded that the white light interferometric fringe pattern of a typical small radius spherical head shows a much higher spacing gradient in both the axial and the circumferential direction than the corresponding fringe pattern

of a large radius spherical head, i.e., the air bearing becomes increasingly more uniform with increasing head radius.

Contour plots of pressure and spacing as predicted by the simulator are shown for a small radius head (19 mm) in Fig. 7, a medium radius head (25 mm) in Fig. 8, and a large radius head (32 mm) in Fig. 9. From the spacing



Figure 10 White light interferometric fringe pattern for a spherical head (taken from R. Tseng [11]).

gradients, we see that the experimental findings of Talke and Tseng [9] are also predicted by the simulator, that is, the simulation also shows a more uniform bearing surface with increasing head radius.

Comparing Figs. 7 through 9, other observations concerning the pressure distribution and film thickness between the tape and rotating head can be made. For all heads, there is a negative pressure at the trailing portion of the head followed by a rather steep gradient to a positive pressure "spike." For small radius heads, the area covered by the positive pressure is roughly the same as the area covered by the negative pressure, but the positive pressure amplitude is considerably larger than the negative amplitude. For the larger radius heads, the positive and negative pressure amplitudes become nearly equal; however, the area covered by the positive pressure becomes larger than that covered by negative pressure. In fact, for the 32-mm head there is an extremely large region of constant positive pressure. The tendency toward larger regions of constant pressure with increasing head radius may account for the tendency toward more uniform spacing. In addition to the spacing gradients becoming less steep with increasing radius, it is also interesting to note that the point of minimum spacing moves toward the trailing portion of the head; this tendency has also been observed experimentally [10, 11].

Quantitative prediction of the flying height is more difficult since in addition to the head and tape parameters one must also consider such things as the surface roughness of the tape and the fact that the tape is not rigidly fixed to the mandrel, but rather floats on an air film [8]. However, comparing the interferometric fringe pattern for a spherical head (Fig. 10), taken from Tseng [11], with the calculated fringe pattern shown in Fig. 9, we see that, for similar parameters, the head-to-tape spacing predicted by the simulator correlates with the experimentally observed spacing. In particular, both experimental and calculated results show fringes of the same shape and size with the point of minimum spacing at the trailing portion of the head. The spacing gradients in both directions are the same for both experimental and calculated results, and the values of the minimum spacing are within 25% of each other. The flying heights obtained by this simulator have been found to be, at worst, of the same order of magnitude as those seen experimentally, and the simulator has also predicted the changes in flying height that accompany various parameter changes.

In general, it has been found that the tape dynamics equations coupled with the Reynolds equation give results which agree well with observed behavior for a rotating spherical head; extensions to other head contours would only require the appropriate changes in Eq. (7).

#### **Acknowledgments**

The coupling procedure used in this simulator was developed jointly with S. Vogel. The author also thanks W. Langlois for the use of several routines relating to the solution of the Reynolds equation. The many helpful suggestions of D. Bogy, F. Talke, and R. Tseng throughout the course of the project are also gratefully acknowledged.

# References and notes

- J. P. Harris, R. S. Rohde, and N. K. Arter, "The IBM 3850 Mass Storage System: Design Aspects," *Proc. IEEE* 63, No. 8, 1171-1176 (1975).
- N. A. Feliss and F. E. Talke, "Capacitance Probe Study of Rotating-Head/Tape Interface," IBM J. Res. Develop. 21, 289-293 (1977).
- D. M. Albrecht, E. G. Laenen, and Chua Lin, "Experiments on the Dynamic Response of a Flexible Strip to Moving Loads," IBM J. Res. Develop. 21, 379-383 (1977).
- D. B. Bogy, H. J. Greenberg, and F. E. Talke, "Steady Solution for Circumferentially Moving Loads on Cylindrical Shells," *IBM J. Res. Develop.* 18, 395-400 (1974).
- 5. The results in this section are taken from an IBM Research Report by D. B. Bogy, H. J. Greenberg, and F. E. Talke.
- A. Burgdorfer, "The Influence of the Molecular Mean-Free Path on the Performance of Hydrodynamic Gas Lubricated Bearings," Trans. ASME Part D (J. Basic Engineering) 81, 94-100 (1959).
- K. J. Stahl, J. W. White, and K. L. Deckert, "Dynamic Response of Self-acting Foil Bearings," *IBM J. Res. Develop.* 18, 513-520 (1974).

- 8. W. A. Michael, "A Gas Film Lubrication Study Part II: Numerical Solution of the Reynolds Equation for Finite Slider Bearings," *IBM J. Res. Develop.* 3, 256-259 (1959).
- F. E. Talke and R. C. Tseng, "Submicron Transducer Spacings in Rotating Head/Tape Interfaces," *IEEE Trans. Magnetics* MAG-12, 725-727 (1976).
- N. A. Feliss, unpublished experimental data, July 1974; IBM Research Division laboratory, 5600 Cottle Road, San Jose, CA 95193.
- R. C. Tseng, unpublished experimental data, 1972-1974;
   IBM General Products Division laboratory, 5600 Cottle Road, San Jose, CA 95193.

Received April 7, 1978; revised August 18, 1978

The author is located at the IBM Research Division San Jose laboratory, 5600 Cottle Road, San Jose, California 95193.